Annals of Biomedical Engineering, Vol. 24, pp. 595–605, 1996
Printed in the USA.

0090-6964/96 $10.50 + .00

A Piconewton Force Transducer and Its Application to Measurement of the Bending Stiffness of Phospholipid Membranes

VOLKMAR HEINRICH and RICHARD E. WAUGH

Department of Biophysics, University of Rochester School of Medicine and Dentistry, Rochester, NY

Abstract—The bending stiffness of a phospholipid bilayer (k_c) was measured by forming thin bilayer cylinders (tethers) from giant phospholipid vesicles. Based on the balance of forces, the tether force was expected to be proportional to the square root of the membrane tension, with a constant of proportionality containing k_c. The membrane tension was controlled via the aspiration pressure in a micropipette used to hold the vesicle. The force on the tether was generated by an electromagnet acting on a paramagnetic bead attached to the vesicle surface. The magnitude of the force was determined from measurements of the magnet current, which was adjusted to maintain the position of the bead. Measurements were performed on vesicles composed of stearoyl-oleoyl-phosphatidylcholine plus 5% (by mole) biotinylated phosphatidylethanolamine to mediate adhesion to streptavidin-coated beads. From each vesicle, tethers were formed repeatedly at different values of the membrane tension. The expected relationship between membrane tension and tether force was observed. The mean value of k_c for 10 different vesicles was 1.17×10^{-19} J (SD = 0.08×10^{-19} J). The precision of these data demonstrates the reliability of this approach, which avoids uncertainties of interpretation and measurement that may be associated with other methods for determining k_c.

Keywords—Magnetic particles, Bilayer membrane, Mechanics, Micromanipulation, Curvature elasticity

INTRODUCTION

To a large extent progress in the biomechanics of cells and subcellular structures such as biomembranes has been confined by the small number of experimental approaches that are available. The method that has accounted for our most detailed knowledge of mechanical properties of cells and membranes is micropipette aspiration. In recent years, the need for alternative approaches to cellular micromechanics has been mainly met by the "optical tweezers" technique employing laser-generated optical traps (2). This technique has provided the possibility of imposing forces in the range of piconewtons, a task that arises in numerous physical and biological applications. Yet options for applying well-known and well-controlled small forces are rather limited (*e.g.*, Ref. 9). In this paper we present an adaptation of a magnetic force transducer developed by Guilford and Gore (14) to apply and measure small forces in a range down to piconewtons. For many experimental purposes, this force transducer provides a low-cost and flexible alternative to optical tweezers.

The main application of magnetic particles in biological research has been their use in magnetic separators. Guilford and coworkers (15) have introduced a technique in which single magnetic beads were attached to leukocytes, and forces generated during cell locomotion were measured. Combining this original work with micromanipulation techniques has provided the basis for the development of our force transducer. Any objects like soft microparticles, biological cells, or even small tissue samples are potentially suitable subjects of study with the apparatus.

A general overview of the experimental setup is the following. The object of investigation is held in a micropipette or otherwise fixed to a micromanipulator on the stage of a microscope. Using antibodies or other adhesive molecules, a paramagnetic bead of spherical shape is attached to it. An electromagnet designed to fit on the microscope stage is positioned with its tip close to the optical path, *i.e.*, the point of observation. In connection with an appropriate force calibration, well-defined forces can be applied to the magnetic bead. The deformation of the specimen at known force is observed microscopically and provides the information needed to characterize the mechanical properties of the material.

In the present paper, the operation of the force transducer is demonstrated with giant phospholipid vesicles. These are artificial, closed bilayer membranes of given lipid composition that form spontaneously in aqueous so-

Acknowledgment—The authors thank Richard G. Bauserman and James Butler for technical assistance, Dr. C. Jeffrey Wang of Spherotech, Inc., for his generosity with bead samples and technical advice, and Philippe Méléard for patiently supplying us with hints for the setup of the vesicle electroformation method. This work was supported in part by a postdoctoral fellowship of the Deutsche Forschungsgemeinschaft, and by the U.S. Public Health Service under NIH grants HL 18208 and HL 31524.

Address correspondence to Dr. Richard E. Waugh, Department of Biophysics, University of Rochester School of Medicine and Dentistry, 601 Elmwood Ave., Rochester, NY 14642.

(Received 22Dec95, Accepted 31Jan96)

lution (1,19,23). They are a preferred model system for establishing the mechanical characteristics of lipid membranes (7). The bending stiffness (k_c) of phospholipid bilayers has raised the particular interest of many research groups (8,13,22,24,26). Its extremely small value is on the order of the thermal energy k_bT, and therefore, it is difficult to measure. In fact, different experimental techniques have produced a rather broad range of k_c values (cf, *e.g.*, Ref. 18). Although our first data are primarily meant to demonstrate the application of the magnetic bead apparatus rather than to answer open questions, the consistency of the measured results indicates that the new method provides for an exceptionally accurate determination of k_c, and so it should provide additional stimulation to the ongoing discussion.

When the bead is pulled away from a vesicle held in a pipette it is typical that the vesicle forms a membrane tether (3). The tether is a thin cylindrical membrane tube that connects the remaining spherical vesicle body with the bead. The main deformation during tether formation bends the initially more or less flat membrane into a very narrow tube, and so tether formation is a good candidate for direct measurement of the membrane bending stiffness. A variety of tether experiments have been carried out and have provided new information about phospholipid bilayers. The earliest measurements based on tether formation provided estimates of k_c and demonstrated its dependence on the cholesterol content in 1-stearoyl-2-oleoyl-sn-phosphatidylcholine (SOPC) membranes (3,28). Subsequently, tether formation was used to make the first (and until now only) measurements of the nonlocal bending modulus, which accounts for the relative stretching of the two monolayers with respect to each other (4,6,31). More recently, tether formation was used to obtain the friction coefficient for movements of the monolayers relative to each other (11,12). With the exception of the work by Evans and Yeung (11), measurement uncertainties in the experimental data have resulted in an undesirably large scatter in the calculated membrane material constants. Refinements in measurement protocols that allow for both variation in applied tethering force and precise measurement of the force represent important advantages of the present method. This has enabled us to determine the force necessary to maintain a tether at a given length as a function of the aspiration pressure applied in the pipette. As will be shown below, this particular measurement provides a very robust method of determining the bending stiffness of lipid bilayers.

MAGNETIC FORCE TRANSDUCER

Figure 1 presents a schematic overview of the basic components of the experimental apparatus. A typical experimental video micrograph is reproduced in Fig. 2. Its essential components are sketched in Fig. 3, where notations used throughout this paper are also given. Figures 2 and 3 show a phospholipid vesicle that is partially aspirated into a glass micropipette. The pipette was mounted on a micromanipulator and could be moved relative to the chamber. A paramagnetic bead was attached to the vesicle. An electromagnet controlled the force that the bead exerted on the vesicle. The vesicle deformation caused by pulling the bead toward the magnet was observed in a light microscope and recorded on videotape.

Since the magnetic field strength depends on the distance from the magnet, all measurements were performed at a fixed distance between the bead and the magnet tip. To keep this distance constant, a computer-controlled feedback system was designed. Video frames were digitized and analyzed at high speed to detect the bead position at any given moment. The current through the magnet was adjusted via a programmable power supply to keep the bead stationary at the desired position. A time average of the current was monitored and saved to disk upon a keystroke. As a backup, a small voltage proportional to the output current of the power supply was encoded into a video signal that was displayed and recorded together with the original image of the experiment.

The feedback system required a fast and reliable way to locate the bead in a video image. The bead-finding algorithm searched for the bead within a small box, the dimensions and initial position of which were set in the beginning of every experiment. Appropriate box dimensions were three to five bead diameters horizontally, *i.e.*, in the direction of the magnet core, and one and a half bead diameters vertically. During the experiment, the box position was constantly updated by placing its center automatically in the most recently measured bead position. Then the next bead-searching cycle was carried out within the relocated box. Only the image framed by this box was read from the digitized video frame. The image was transformed into a binary image with a gray value threshold that was set to separate the bead from the background. The bead position was determined as the center of all bead pixels.

After the actual experiment an independent force calibration was carried out that gave the force acting on the bead as a function of the current through the magnet. It was based on Stokes' law, using the velocity at which the free bead moved in the magnetic field. The velocity was measured at the same position at which the bead had been kept stationary in the experiment.

Both experiment and calibration were done in the same aqueous solution at a sufficient height (at least 20 bead diameters) above the chamber bottom to minimize wall effects. There were no magnetic beads in the measurement chamber other than the one attached to the vesicle. The

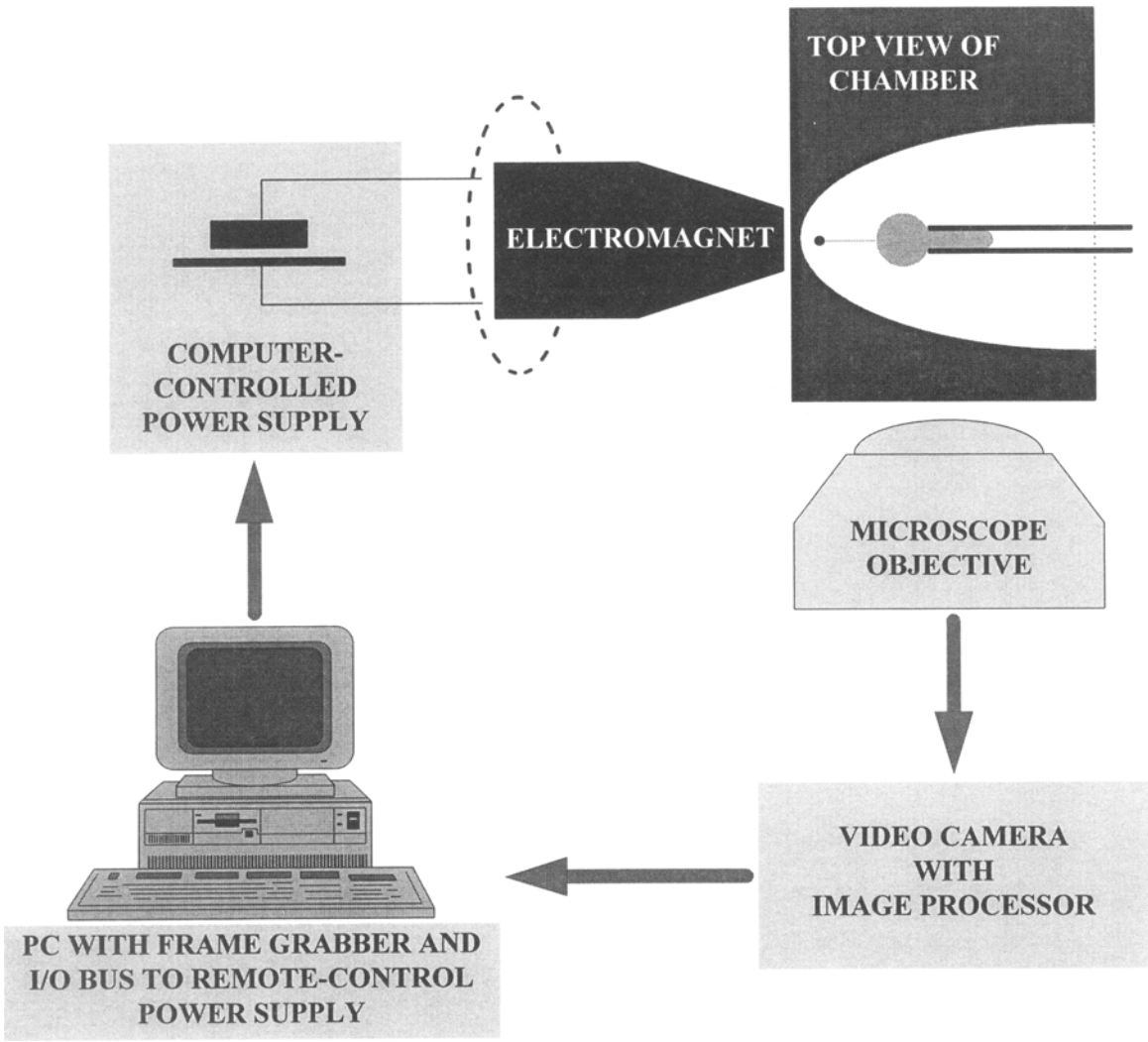

FIGURE 1. Schematic overview of the experimental apparatus. A paramagnetic bead is attached to the surface of a phospholipid vesicle, the membrane tension of which is controlled via the aspiration pressure applied in a micropipette (cf. Fig. 3). The tethering force exerted by the bead is generated by an electromagnet mounted on the stage of a microscope. A fast computer algorithm identifies the bead in digitized video images (cf. Fig. 2) and adjusts the magnet current to maintain the bead position fixed. For more details see the text.

bead density was small enough that even at the lowest magnetic fields applied, the attached bead did not move out of the focal plane because of gravity. The current was not allowed to exceed a certain upper limit, which prevented the water-cooled magnet from heating.

Different magnets and experimental chambers have been designed and built in our laboratory for use in a variety of applications. Within a given experimental setup, the pulling force was varied over a wide range by changing the current through the magnet. Moreover, for different purposes this range can easily be broadened by varying the beads' magnetic properties or simply changing the distance between the magnet tip and the measurement position. Of course, such changes require a new force calibration.

EXPERIMENTAL PROCEDURE

All observations were made with a Nikon Diaphot inverted light microscope. The experimental setup required an easily accessible microscope stage and long working distance optics. Pipette-aspirated vesicles are best observed using Hoffman modulation contrast. For a high success rate of the bead-finding algorithm, an even background in the video image was essential. Background subtraction and contrast enhancement were performed using an Argus image processor (Hamamatsu, Bridgewater, NJ, USA) in combination with a sensitive Hamamatsu CCD camera to obtain images with low background and high clarity (Fig. 2). These images were digitized (EZ Vision frame board; Data Translation, Peabody, MA, USA) and

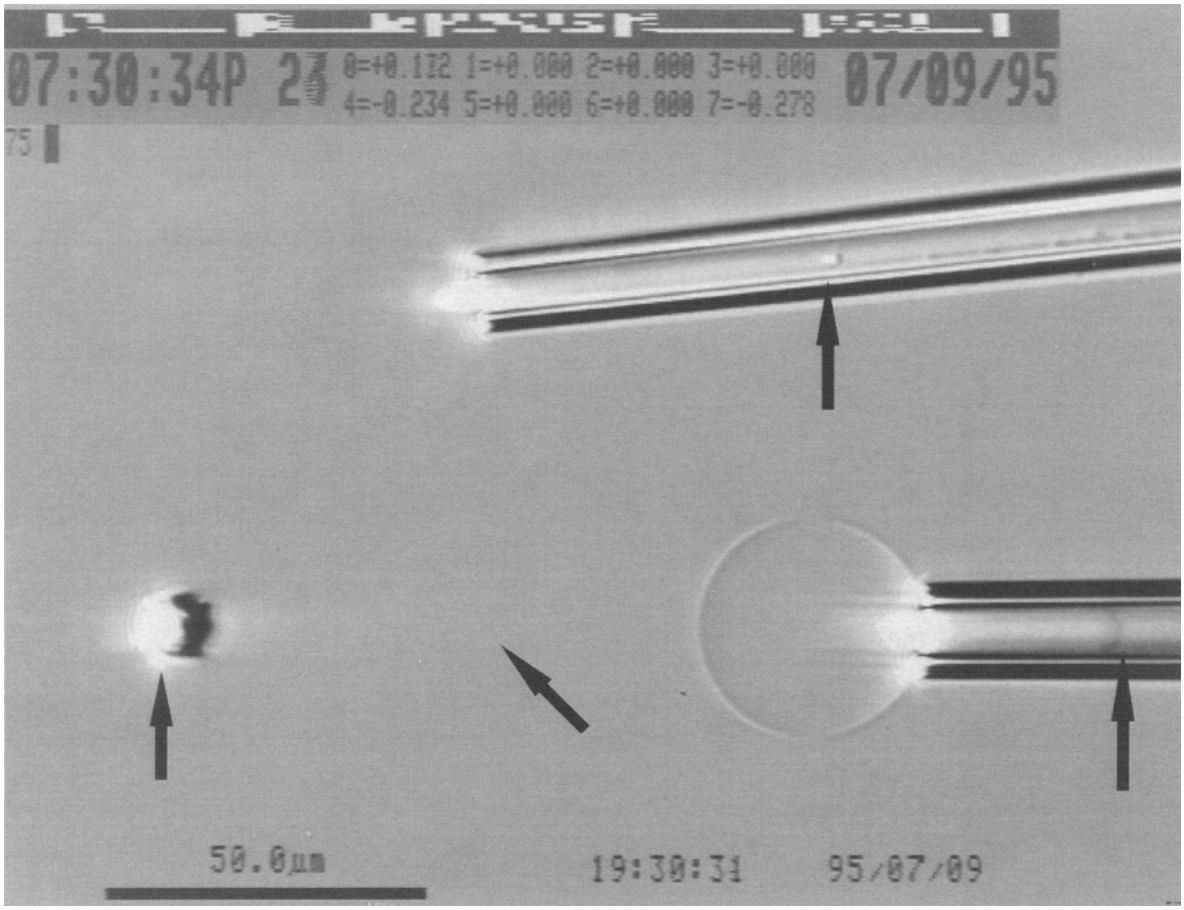

FIGURE 2. Video micrograph of a typical experiment. Large-sized vesicles as well as background subtraction and contrast enhancement provided the high-quality images needed for the bead-finding algorithm. The bead (lower left) and the projection of the vesicle membrane into the pipette (lower right) are indicated by vertical arrows. The membrane tether connecting bead and vesicle (location indicated by the diagonal arrow) is too small to be resolved by light microscopy. In addition to the vesicle pipette, a reference pipette holding a small particle (indicated by the uppermost vertical arrow) was used to monitor and correct for small drifts in zero pressure. Bar = 50.0 µm.

analyzed by a computer program that also controlled the power supply for the magnet (Hewlett Packard, model 6655A) via an HPIB interface.

Phospholipid vesicles were made from a lipid mixture of SOPC (Avanti Polar Lipids, Birmingham, AL, USA) with 5% biotin-X-DHPE (*N*-((6-(biotinoyl)amino)hexanoyl)-1,2-dihexacanoyl-sn-glycero-3-phosphoethanolamine; Molecular Probes, Eugene, OR, USA), which had been dissolved in chloroform/methanol (2:1) at a concentration of 0.25 mg/ml. Vesicles were prepared using a modified version of the electroformation method of Angelova *et al.* (1). The lipid (~40 µl) was laid down on a pair of cylindrical electrodes (thick platinum wire) and vacuum dried for 2 hours. The electrodes were placed in a chamber that was then cautiously filled with 80 mM sucrose solution. An alternating electric field of ~1 kV/m was applied, starting at a frequency of 10 HZ. Vesicle growth could be observed directly under the microscope. After 1 hour, the frequency was reduced in several steps to 1 HZ. At the same time, the amplitude usually needed to be decreased stepwise to a final value of ~0.2 kV/m to maintain smooth movements of the vesicles. When a satisfactory number of vesicles had formed, the chamber was gently flushed and the vesicles were harvested into a storage container. The vesicles prepared in this way were usually large, with diameters up to 150 µm, and the majority of them appeared to be unilamellar.

In an experiment, the vesicle suspension was diluted ~1:1 in 85 mM glucose solution containing 1.15 mOsm phosphate-buffered saline and 0.3% bovine serum albumin. Paramagnetic beads coated with streptavidin (Spherotech, Libertyville, IL, USA) were washed and suspended in the same 85 mM glucose solution in a separate chamber. A single vesicle was aspirated into a glass micropipette and then transferred to the bead chamber. Transfers were carried out inside a separate pipette that had a U-shaped tip and a diameter big enough to accommodate the vesicle held in the vesicle pipette. The transfer

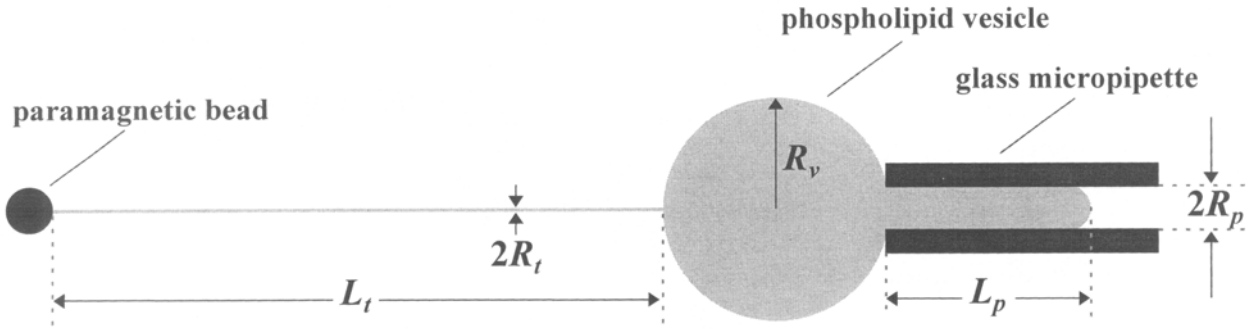

FIGURE 3. Sketch of vesicle-bead pair and pipette with notation of geometric parameters. Aligning magnet core and pipette in the beginning of each experiment provided the rotational symmetry that is the geometric basis for the model used to derive the equilibrium equations.

pipette entered the chamber from the same side as the vesicle pipette and was mounted on its own micromanipulator. In the bead chamber, a single bead was stuck to the vesicle, and then the vesicle-bead pair was transferred to the measurement chamber containing 90 mM sucrose solution (with 1.15 mOsm phosphate-buffered saline and 0.3% bovine serum albumin). To eliminate evaporation, the opening of the measurement chamber was placed inside a larger, environmental chamber that was kept under high humidity by using a stream of water-saturated nitrogen.

The force needed to maintain a tether of given length was measured as a function of the aspiration pressure in the pipette. At each pressure value, a tether was formed by pulling the magnetic bead toward the magnet. After a few initial oscillations, the tether was maintained at a stable length for at least 20 sec. The average current applied to the magnet during this period was saved, and the magnet was then turned off. Removal of the magnetic force allowed the tether to be reincorporated into the body of the vesicle. After reincorporation, the aspiration pressure was increased (or decreased) to the next value, and a new tether was formed by turning the magnet on again. In all measurements, zero pressure was controlled by holding a small particle in a separate reference pipette mounted on a third micromanipulator.

After finishing the measurements, the bead was detached from the vesicle and picked up in a pipette. It was moved away from the magnet to the edge of the field of view on the video monitor and held there at zero pressure close to the pipette tip. The magnet was turned on at a given current, and the motion of the free bead through the solution toward the magnet was recorded. Once the bead had passed the position at which it had been held stationary when pulling tethers, the magnet was turned off and the bead was picked up again. This was repeated about five times for each value of the current.

Pipette diameters were determined by measuring the insertion depth of a glass probe, the diameter of which had been measured as a function of distance from the tip in an electron microscope. The ratio of the change in insertion depth to the change in diameter was approximately 10. Thus, assuming the insertion depth can be measured to an accuracy of ± 0.5 μm, the pipette diameter was determined to an accuracy of ± 0.05 μm.

ANALYSIS OF TETHER EQUILIBRIUM

The mathematical model underlying the interpretation of the measurements follows closely the analysis in Božič *et al.* (4). Geometrically, all parts of the vesicle were assumed to be either cylindrical (tether, part of the projection of the vesicle in the pipette) or spherical (vesicle body, hemispherical cap of the projection). For the notation of geometric parameters see Fig. 3.

The equilibrium equations were derived by minimizing the system's total energy. Details of the derivation are given in Appendix 1. The resulting relationship between the force f exerted by the magnetic bead and the membrane tension τ takes the form

$$f = 2\pi\sqrt{2k_c\tau} + \frac{4\pi^2 k_r}{A_0}(L_t - L_t^*), \qquad (1)$$

where k_c and k_r are the local and the nonlocal bending moduli, respectively. The tether length L_t is defined in Fig. 3. The meaning of L_t^* is given in Appendix 1. Its value was assumed to be constant for a given vesicle. The unstressed membrane area A_0 is calculated by applying the conditions for the reference state to Eq. A1.2 (cf. Appendix 1). The isotropic membrane tension τ is formally defined as

$$\tau = \frac{R_v R_p}{2(R_v - R_p)}\Delta p. \qquad (2)$$

For a given vesicle, τ is proportional to the aspiration pressure Δp that is applied in the pipette. The geometrical quantities entering the expression for τ are the pipette radius R_p and the vesicle radius R_v.

The result given by Eq. 1 illustrates the advantage of

the measurement of f as a function of τ (*i.e.*, of Δp) for the determination of the bending stiffness k_c. First of all, the area expansivity modulus K (cf. Appendix 1) does not enter Eq. 1 at all, *i.e.*, this measurement is independent of the membrane expansivity. Furthermore, the slope of a linear fit to the representation of f as a function of the square root of τ contains exclusive information about k_c. This information does not involve L_t, which means that the measurement is also independent of the tether length. As long as the vesicle geometry in the experiment is consistent with the model's geometry, Eq. 1 may be used to interpret the data. This also avoids the experimental inconveniences that occur in the formation of very long tethers. Such long tethers are needed to measure resolvable changes in the projection length L_p (see Fig. 3), which is the basis for an alternative method for calculating k_c (31), or to establish the contribution of nonlocal bending effects to the membrane properties. From the present measurement the nonlocal bending modulus k_r is not accessible, because the intercept of the fitted straight line also contains, besides k_r, the unknown quantity L_t^*. The determination of k_r requires measurements at significantly different tether lengths and (for technical reasons) is beyond the scope of this work.

RESULTS

Figures 4 to 6 illustrate the main steps in obtaining the bending stiffness from the measurements. Original data of a typical experiment are shown in Fig. 4. In the depicted series, a tether was pulled from the same vesicle about 45 times, first at increasing and then at decreasing aspiration pressures. Naturally, while the automated feedback system maintained a tether at final length, the computer-controlled current through the magnet exhibited small fluctuations as a response to small movements of the bead. Bead displacements from the measurement position were usually no more than 2 pixels on the video monitor in either direction. However, the small current fluctuations made it necessary to take the time average of the current.

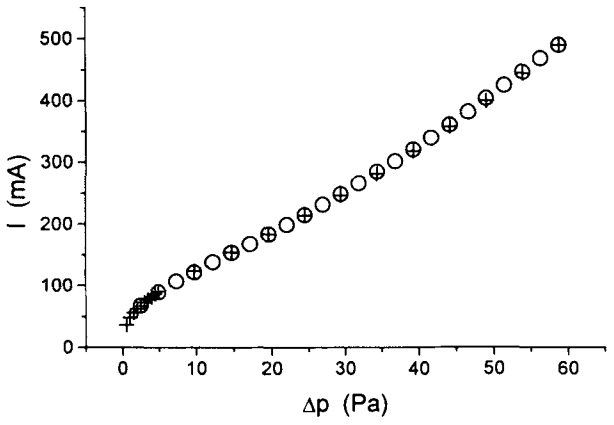

FIGURE 4. Example measurement of the magnet current *I* necessary to maintain a fixed bead position *versus* aspiration pressure Δp applied in the pipette. A new tether was formed for each data point, and it was reincorporated into the vesicle body after saving the current. For this case, the vesicle radius was 18.8 μm and the pipette radius was 4.2 μm. Each value of the current is the average current of ~20 sec, during which the tether length was stable. Measurements of the current were done successively at increasing (○) and then decreasing (+) pressure steps to check for reversibility.

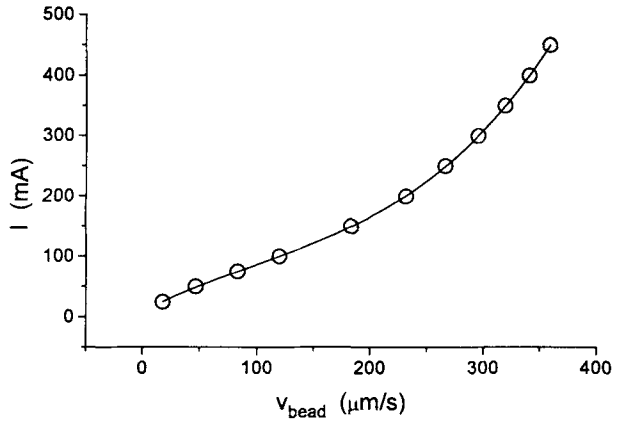

FIGURE 5. Force calibration curve for the bead that was used in the measurements of Fig. 4. The motion of the free bead in the magnetic field had been monitored for different field strengths, and the bead velocity v_{bead} was plotted on the *x* axis of this graph with the magnet current *I* on the *y* axis. In this representation, the data points could be very well modeled by a third-order polynomial: $I = 1.062 \times 10^{-5} v^3 - 0.0031 v^2 + 0.9832v + 9.0255$ (solid curve).

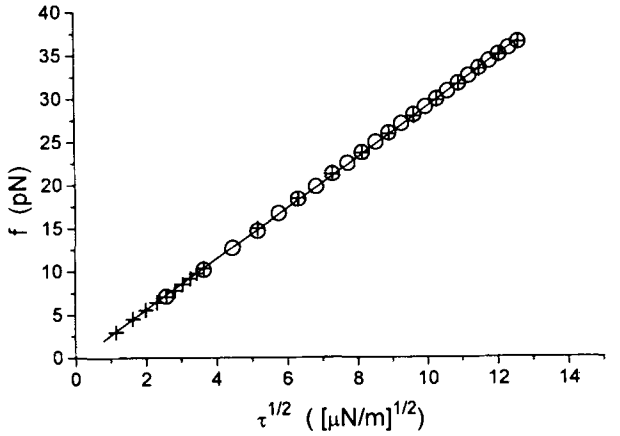

FIGURE 6. Linear dependence of the tethering force *f* on the square root of the membrane tension $\tau^{1/2}$. Data points correspond to those in Fig. 4. The tension τ was obtained from the aspiration pressure Δp using Eq. 2. The values of the current *I* (Fig. 4) were first converted into bead velocities using the calibration curve (Fig. 5), and the force *f* was then calculated from the velocity by Stokes' law (Eq. 3). Separate linear regressions were done for the $f = f(\tau^{1/2})$ data obtained at increasing and decreasing pressures. The resulting straight lines had slopes of 2.929 and 2.927, respectively. The slope of these straight lines contains the square root of the bending stiffness k_c (cf. Eq. 1).

For this, bead position and current during the most recent 40 sec were displayed graphically on the computer screen. When both had been stable for 20 sec, the average current was calculated for this time interval and saved to disk. It is this average current that is shown in Fig. 4 as a function of the aspiration pressure. The measurements of this series took about 25 min. It can be seen from Fig. 4 that the data of the later measurements at decreasing pressure steps follow the same curve as the earlier ones obtained at increasing aspiration pressures. Thus, no observable long-term effects or hysteresis occurred during the experiment.

Figure 5 shows the force calibration curve for the bead that was used to obtain the data in Fig. 4. The bead velocity v_{bead} was determined by measuring frame by frame the position of the free bead moving in the magnetic field. Since the magnetic force increases slightly when the bead moves toward the magnet, the distance-time relation for the bead movement is not strictly linear. It could be well modeled, however, as homogeneously accelerated motion and fit by a second-order polynomial. The velocity was obtained as the derivative of this polynomial with respect to time, taken at the measurement position. At each current, between four and eight measurements of the velocity were carried out. The resulting average speed was plotted on the x axis of Fig. 5, with the current on the y axis. A third-order polynomial fit to the measured data for the current I as a function of the bead velocity v_{bead} yielded very satisfactory agreement in all calibrations.

As a first step toward replacing the recorded current by a force, the velocity v_{bead} was calculated for each value of the current by solving the third-order equation obtained from the calibration. The force f that the bead exerted on the vesicle at a given current was then calculated from the velocity using the expression for the Stokes' drag on a spherical particle moving in a fluid:

$$f = 6\pi R_{bead}\eta v_{bead}, \tag{3}$$

where R_{bead} is the radius of the bead and η is the viscosity of the sucrose solution. (Measurements of the viscosity using a capillary viscometer showed $\eta = 1.065 \times 10^{-3}$ N · s/m^2.) Using the data of Fig. 4 and the calibration of Fig. 5, the force f is shown in Fig. 6 as a function of the square root of the tension τ defined in Eq. 2. The dependence is clearly linear, as predicted by Eq. 1. Linear regressions were done separately for the data at increasing and decreasing pressure, respectively, and yielded two practically identical straight lines. The calculation of the bending stiffness k_c from the slope of the linear fit is straightforward (Eq. 1). For the example shown in Fig. 6 one obtains $k_c = 1.23 \times 10^{-19}$ J.

Measurements were performed on 10 vesicles with vesicle radii R_v (cf. Fig. 3) ranging from 15 to 30 μm and tether lengths L_t between 25 and 315 μm. Pipette radii were between 3.6 and 5.2 μm. For every vesicle-bead pair, the measurements consisted of at least two series to check repeatability, with the aspiration pressure first increasing and then decreasing in each series. The overall number of data points, *i.e.*, of tethers pulled, was about 530. Forces applied covered an overall range from 3 to 43 piconewtons, with bead radii between 3 and 6.2 μm. The average value of the bending modulus obtained from these measurements was $k_c = 1.17 \times 10^{-19}$ J, with a standard deviation of 0.08×10^{-19} J.

DISCUSSION

A variety of bead sizes, different-sized vesicles, and different-sized pipettes were used in this study, yet the measurements have resulted in exceptionally consistent values of k_c. It should be emphasized that both the original data, *i.e.*, the current I measured as a function of the aspiration pressure Δp (cf. Fig. 4), as well as the force-calibration curve (cf. Fig. 5), were obtained from independent measurements. In both cases the measured data showed a nonlinear behavior. However, when they were combined to give the force f as a function of the square root of the membrane tension $\tau^{1/2}$, the resulting data points aligned to represent an almost ideal linear dependence (cf. Fig. 6). This dependence corresponds very well to the theoretically predicted behavior, giving a high level of confidence that the analysis of the problem properly accounts for the most important physical aspects of the process, and so provides an accurate determination of the bending stiffness.

The present method has several substantial advantages over previously published techniques of measuring the bending stiffness. First of all, the only essential deformation is a change in the tether radius R_t resulting from a pressure step in the pipette. Thus, the membrane is bent successively into tubes of different diameters. Since the force necessary for this deformation is known, this experiment provides a direct mechanical measurement of the work required to change the curvature of the circumference of the tether. Furthermore, the measurement of the pulling force f as a function of the membrane tension τ is independent of the membrane expansivity K (see Appendix 1) as well as of the projection length L_p (cf. Fig. 3), which greatly reduces measurement uncertainties.

Despite the consistency of values obtained for k_c with this new approach, there are some uncertainties that must be considered when evaluating the present results. First, there may be systematic errors in the k_c values because of errors in the calibration. In particular, we note the dependence of the calibration on an accurate measure of the bead diameter, an accurate measure of the solution viscosity, and on the applicability of Stokes' law to the used beads, which have a rather rough surface and not always an ideal spherical shape. However, given the variety of

beads used, each of these possible errors should affect the measurements to a different extent in different experiments. Taking into account the smallness of the standard deviation of the final result, we expect the overall error from these uncertainties not to be significantly larger than the standard deviation itself (see Appendix 2). Second, it should be noted that it is necessary to use some percentage of biotinylated lipid to effect adhesion between the bead and the vesicle during the experiment. The extent to which the presence of biotinylated lipid affects the properties of the membrane is unknown and should be the subject of future studies. Assuming that the effect of the biotin lipid on the mechanical properties of the membrane is small, the k_c value of a pure SOPC bilayer should not significantly differ from the value presented here.

In addition to the relationship between force and membrane tension, for some vesicles, measurements were made of changes in the projection length L_p during tether formation at different aspiration pressures. Such measurements provide another, independent way to determine k_c. However, the measurements are technically more difficult, because long tethers are necessary to obtain detectable changes in L_p. But even at moderate tether lengths, L_p changes were only a few video pixels at higher aspiration pressures in the present experiments, and so this measurement had a much lower resolution than the measurement presented above. Indeed, when the same mathematical model (Appendix 1) was adapted to this experimental situation, its predictions were in much worse agreement with the measured data than the tension-force data. Even so, the scatter of resulting k_c values (between 1.05×10^{-19} J and 1.79×10^{-19} J) was larger than expected, taking into account the method's resolution. The scatter in the data can be attributed to larger-than-expected changes in projection length during tether formation at increasing aspiration pressures. One possible explanation might be the existence of nonbilayer structures or very small membrane blebs that are not detectable in the light microscope. It is possible that these structures were "pulled out" during tether formation or at sufficiently high aspiration pressures, which could lead to additional changes in the projection length without significantly affecting the force necessary to maintain a tether. The effect appeared to be irreversible within the relatively short measurement time, and so it could not be interpreted in terms of an "entropic tension" caused by micro-undulations of the bilayer (8). On the contrary, the observations seem to support the hypothesis of an "anomalous roughness" superstructure postulated by Helfrich (18). However, so far the few incidental observations allow at most speculation, and more experiments are needed to study this behavior systematically.

Most of the published k_c values are estimated from measurements of thermally driven fluctuations of the vesicle surface and are based on theoretical models that describe the real physical fluctuation process to varying degrees of accuracy (8,13,26,27). The values for the bending stiffness of SOPC bilayers obtained from these experiments are generally smaller than our result. However, these values could be in error for a number of reasons. An essential uncertainty is the theoretical model for the analysis of fluctuations. It is usually based on a second-order expansion of the model quantities in terms of the deviation from a sphere. It has been shown before that this expansion does not properly reproduce the diversity of equilibrium shapes of vesicles obtained from more general approaches (16). Furthermore, it can be shown that close to so-called symmetry breaking points in the phase diagram of equilibrium shapes (17,25), the vesicle surface exhibits critical fluctuations that cannot be interpreted in terms of the second-order model. Indeed, very recently observations of large vesicle shape fluctuations of this kind have been reported (5). In an experiment, a vesicle with an equilibrium shape that is in a critical region of the phase diagram will certainly show more pronounced shape fluctuations. The probability that such a vesicle will be picked by the observer is rather high. Naturally, the apparent bending stiffness of such a vesicle will be smaller if calculated on the basis of the traditional model. In addition, in both the theory used to analyze fluctuations of free vesicles as well as in the fluctuation-based "effective tension" interpretation of low-pressure aspiration experiments (8), the contribution of nonlocal bending effects and the proper inclusion of constraints are questions that do not yet appear to be completely answered.

Considering these uncertainties, a direct measurement of the relationship between deformation and imposed force seems to be a preferable way to determine the bending stiffness of membranes. The magnetic force transducer has enabled us to perform this measurement with an exceptional accuracy. The above results demonstrate the capability of the force transducer to apply and measure extremely small forces with a resolution of a fraction of a piconewton. First test experiments have shown that the force transducer can also be used in a similar way to establish the mechanical properties of red blood cell membranes. The apparatus presented in this paper can be adapted to a large variety of other tasks, and so it can certainly help to gain new insight in a number of problems in microbiomechanics. For example, there has been considerable discussion in the literature regarding relationships between the bending stiffness k_c and the membrane area compressibility modulus K (10,29,30). Although the present data are not sufficient to provide a critical test of these predictions (because only one type of membrane is tested), we can begin to assess what models are consistent with the present findings. The value of K of SOPC membranes has been well determined by at least two different

groups to be between 190 and 200 mN/m (8,21). Measurements of this parameter in our laboratory (unpublished) also confirm this value. Using a value for K of 200 mN/m and a value for k_c of 1.2×10^{-19} J, and assuming that the elastic contributions arise equally from each of the constituent monolayers of the bilayer, we find that the individual monolayers could be modeled as homogeneous layers, each monolayer having a thickness of 2.7 nm (30). Taking the sum of two monolayers, we get a value for the total membrane thickness of 5.4 nm, which is quite close to the membrane thickness determined from X-ray diffraction measurements (20). Clearly, other models could also fit these values of K and k_c, and further experimentation on membranes of different thickness and composition will be needed to critically test these relationships.

REFERENCES

1. Angelova, M. I., S. Soléau, Ph. Méléard, J. F. Faucon, and P. Bothorel. Preparation of giant vesicles by external AC electric fields. Kinetics and applications. *Prog. Colloid. Polym. Sci.* 89:127–131, 1992.
2. Ashkin, A., and J. M. Dziedzic. Optical trapping and manipulation of viruses and bacteria. *Science* 235:1517–1520, 1987.
3. Bo, L., and R. E. Waugh. Determination of bilayer membrane bending stiffness by tether formation from giant, thin-walled vesicles. *Biophys. J.* 55:509–517, 1989.
4. Božič, B., S. Svetina, B. Žekš, and R. E. Waugh. The role of lamellar membrane structure in tether formation from bilayer vesicles. *Biophys. J.* 61:963–973, 1992.
5. Döbereiner, H.-G., E. Evans, U. Seifert, and M. Wortis. Spinodal fluctuations of budding vesicles. *Phys. Rev. Lett.* 75:3360–3363, 1995.
6. Evans, E. A. Minimum energy analysis of membrane deformation applied to pipet aspiration and surface adhesion of red blood cells. *Biophys. J.* 30:265–284, 1980.
7. Evans, E., and D. Needham. Physical properties of surfactant bilayer membranes: Thermal transitions, elasticity, rigidity, cohesion, and colloidal interactions. *J. Phys. Chem.* 91:4219–4228, 1987.
8. Evans, E., and W. Rawicz. Entropy-driven tension and bending elasticity in condensed-fluid membranes. *Phys. Rev. Lett.* 64:2094–2097, 1990.
9. Evans, E., K. Ritchie, and R. Merkel. Sensitive force technique to probe molecular adhesion and structural linkages at biological interfaces. *Biophys. J.* 68:2580–2587, 1995.
10. Evans, E. A., and R. Skalak. Mechanics and thermodynamics of biomembranes. *CRC Crit. Rev. Bioeng.* 3:181–418, 1979.
11. Evans, E., and A. Yeung. Hidden dynamics in rapid changes of bilayer shape. *Chem. Phys. Lipids* 73:39–56, 1994.
12. Evans, E., A. Yeung, R. Waugh, and J. Song. Dynamic coupling and nonlocal curvature elasticity in bilayer membranes. In: *The Structure and Conformation of Amphiphilic Membranes,* edited by R. Lipowsky, D. Richter, and K. Kremer. Berlin, Heidelberg: Springer-Verlag, 1992, pp. 148–153.
13. Faucon, J. F., M. D. Mitov, P. Meleard, I. Bivas, and P. Bothorel. Bending elasticity and thermal fluctuations of lipid membranes. Theoretical and experimental requirements. *J. Phys. France* 50:2389–2414, 1989.
14. Guilford, W. H., and R. W. Gore. A novel remote-sensing isometric force transducer for micromechanics studies. *Am. J. Physiol.* 263:C700–C707, 1992.
15. Guilford, W. H., R. C. Lantz, and R. W. Gore. Locomotive forces produced by single leukocytes in vivo and in vitro. *Am. J. Physiol.* 268:C1308–C1312, 1995.
16. Heinrich, V., M. Brumen, R. Heinrich, S. Svetina, and B. Žekš. Nearly spherical vesicle shapes calculated by use of spherical harmonics: Axisymmetric and nonaxisymmetric shapes and their stability. *J. Phys. France* 2:1081–1108, 1992.
17. Heinrich, V., S. Svetina, and B. Žekš. Nonaxisymmetric vesicle shapes in a generalized bilayer-couple model and the transition between oblate and prolate axisymmetric shapes. *Phys. Rev. E* 48:3112–3123, 1993.
18. Helfrich, W. Tension-induced mutual adhesion and a conjectured superstructure of lipid membranes. In: *Handbook of Biological Physics,* Vol. 1, edited by R. Lipowsky and E. Sackmann. Amsterdam: Elsevier Science B.V., 1995, pp. 691–721.
19. Lipowsky, R. The conformation of membranes. *Nature* 349: 475–481, 1991.
20. McIntosh, T. J., and S. A. Simon. Hydration force and bilayer deformation: A reevaluation. *Biochemistry* 25:4048–4066, 1986.
21. Needham, D., and R. S. Nunn. Elastic deformation and failure of lipid bilayer membranes containing cholesterol. *Biophys. J.* 58:997–1009, 1990.
22. Niggemann, G., M. Kummrow, and W. Helfrich. The bending rigidity of phosphatidylcholine bilayers: Dependences on experimental method, sample cell sealing and temperature. *J. Phys. France* 5:413–425, 1995.
23. Reeves, J. P., and R. M. Dowben. Formation and properties of thin-walled phospholipid vesicles. *J. Cell. Physiol.* 73:49–60, 1969.
24. Sackmann, E. Physical basis of self-organization and function of membranes: Physics of vesicles. In: *Handbook of Biological Physics,* Vol. 1, edited by R. Lipowsky and E. Sackmann. Amsterdam: Elsevier Science B.V., 1995, pp. 213–304.
25. Seifert, U., K. Berndl, and R. Lipowsky. Shape transformation of vesicles: Phase diagram for spontaneous-curvature and bilayer-coupling models. *Phys. Rev. A* 44: 1182–1202, 1991.
26. Schneider, M. B., J. T. Jenkins, and W. W. Webb. Thermal fluctuations of large cylindrical phospholipid vesicles. *Biophys. J.* 45:891–899, 1984.
27. Servuss, R. M., W. Harbich, and W. Helfrich. Measurement of the curvature-elastic modulus of egg lecithin bilayers. *Biochim. Biophys. Acta* 436:900–903, 1976.
28. Song, J. B., and R. E. Waugh. Bending rigidity of SOPC membranes containing cholesterol—brief communication. *Biophys. J.* 64:1967–1970, 1993.
29. Svetina, S., and B. Žekš. Elastic properties of closed bilayer membranes and the shapes of giant phospholipid vesicles. In: *Handbook of Nonmedical Applications of Liposomes,* Vol. 1, edited by D. D. Lasic, and Y. Barenholz. Boca Raton, New York, London, Tokyo: CRC Press, 1996, pp. 13–42.
30. Waugh, R. E., and R. M. Hochmuth. Mechanical equilibrium of thick hollow liquid membrane cylinders. *Biophys. J.* 52:391–400, 1987.

31. Waugh, R. E., J. Song, S. Svetina, and B. Žekš. Monolayer coupling and curvature elasticity in bilayer membranes by tether formation from lecithin vesicles. *Biophys. J.* 61: 974–982, 1992.

APPENDIX 1

All geometric parameters are defined in Fig. 3. Assuming that the vesicle is composed exclusively of cylindrical and spherical parts, the vesicle volume V is approximated by

$$V = \frac{4}{3}\pi R_v^3 + \pi R_p^2 L_p - \frac{\pi}{3}R_p^3, \tag{A1.1}$$

where the small volume of the tether has been neglected ($R_t \ll R_v$). The membrane area A is

$$A = 4\pi R_v^2 + 2\pi R_p L_p + 2\pi R_t L_t - \pi R_p^2. \tag{A1.2}$$

Taking into account that the membrane consists of two monolayers, and assuming that these have a constant separation distance h ($h \ll R_v$), the difference between monolayer areas ΔA is expressed as

$$\Delta A = 2\pi h(4R_v + L_p + L_t + R_p). \tag{A1.3}$$

As a reference state we will take a vesicle without a tether (no pulling force, $L_t = 0$) that is aspirated at the smallest pressure that produces a stable projection and spherical vesicle body. Geometric quantities referring to this state are denoted by the subscript 0. As an exception, ΔA_0 is defined for isolated, unstretched monolayers and is unknown. Denoting $\Delta L_p = L_p - L_{p_0}$, one may write

$$V - V_0 = \frac{4}{3}\pi(R_v^3 - R_{v_0}^3) + \pi R_p^2 \Delta L_p \tag{A1.4}$$

$$A - A_0 = 4\pi(R_v^2 - R_{v_0}^2) + 2\pi R_p \Delta L_p + 2\pi R_t L_t. \tag{A1.5}$$

The volume of the vesicle is assumed to be constant, *i.e.*, $V = V_0$. This constraint is used to eliminate ΔL_p from all following expressions, using Eq. A1.4 in the form

$$\Delta L_p = \frac{4}{3}\frac{R_{v_0}^3 - R_v^3}{R_p^2}. \tag{A1.6}$$

Thus, Eq. A1.5 becomes

$$A - A_0 = \frac{8}{3}\pi\frac{R_{v_0}^3 - R_v^3}{R_p} + 4\pi(R_v^2 - R_{v_0}^2) + 2\pi R_t L_t. \tag{A1.7}$$

To calculate the difference $\Delta A - \Delta A_0$, one has to take into account the observation that during tether formation, changes in the tether length L_t are much larger than changes in the other variables entering Eq. A1.3. We may treat these variables as constants and collect them together with ΔA_0 in a new constant L_t^* that is defined in such a way that

$$\Delta A - \Delta A_0 = 2\pi h(L_t - L_t^*). \tag{A1.8}$$

It is assumed that the vesicle membrane is in equilibrium when the tether is held at a stable length. At equilibrium the total energy of the system has a minimum. The total energy is the sum of two membrane bending energies, the energy of the membrane expansion, the work done by the aspiration pressure, and the work done by the pulling force of the bead (4).

Neglecting small or constant energy contributions, we first obtain the local bending energy as

$$W_b = \pi k_c \frac{L_t}{R_t}, \tag{A1.9}$$

where k_c is the local bending modulus. Using Eq. A1.8, the nonlocal bending energy is calculated as

$$W_r = \frac{k_r}{2A_0}\left(\frac{\Delta A - \Delta A_0}{h}\right)^2 = \frac{2\pi^2 k_r}{A_0}(L_t - L_t^*)^2, \tag{A1.10}$$

with the nonlocal bending modulus k_r. Denoting the area expansivity modulus by K, the energy of membrane expansion is

$$W_t = \frac{K}{2A_0}(A - A_0)^2. \tag{A1.11}$$

The work done by the aspiration pressure Δp is given by

$$W_p = -\pi R_p^2 \Delta L_p \Delta p = \frac{4}{3}\pi(R_v^3 - R_{v_0}^3)\Delta p, \tag{A1.12}$$

and, finally, the work of the axial force f exerted by the magnetic bead is calculated as

$$W_f = -fL_t. \tag{A1.13}$$

The equilibrium equations are derived by minimizing the total energy:

$$W_{tot} = W_b + W_r + W_t + W_p + W_f = W_{tot}(R_v, L_t, R_t). \tag{A1.14}$$

At a minimum, the partial derivatives of W_{tot} with respect to the independent variables R_v, L_t, and R_t have to vanish. The resulting three equations can be combined into the following pressure-force relation:

$$f = 2\pi\sqrt{\frac{k_c R_v R_p}{R_v - R_p}}\Delta p + \frac{4\pi^2 k_r}{A_0}(L_t - L_t^*). \tag{A1.15}$$

Finally, Eq. 1 is obtained from Eq. A1.15 by introducing the tension τ defined in Eq. 2.

APPENDIX 2

In this appendix we consider the possible sources of error in our measurements as a guide to other investigators who might wish to use this technique. The most significant uncertainties come from relating the measured current to the actual force on the bead, and from the resolution limits of light microscopy. To consider the possible errors introduced into the calculated value of the bending stiffness, we write k_c in the form

$$k_c = 9(R_{bead})^2 \eta^2 \left(\frac{1}{R_p} - \frac{1}{R_v}\right)\left(\frac{dv_{bead}(I)}{d\sqrt{\Delta p}}\right)^2. \quad \text{(A2.1)}$$

The error contribution of each measured quantity is expected to be the product of the partial derivative of k_c with respect to this quantity times the uncertainty in the measurement of the quantity itself. For example, the expected error in k_c (δk_c) resulting from a measurement error in the bead radius (δR_{bead}) is given by

$$\left(\frac{\delta k_c}{k_c}\right)_{R_{bead}} = \frac{2\delta R_{bead}}{R_{bead}}. \quad \text{(A2.2)}$$

As expected, because R_{bead} enters Eq. A2.1 as the square, the contribution of uncertainties in the measurement of R_{bead} to the relative error in k_c is twice the relative error in R_{bead}. Thus, the most significant errors are likely to come from errors in the value of the solution viscosity (which may vary significantly with temperature or solute concentration) and from measurements of the bead radius. (We note that although the slope also enters as the square, the uncertainty in the slope is relatively small (Fig. 6).) Errors in the vesicle radius (~2.5%) and errors in the pipette radius (~1%) enter only to first order and are significantly smaller than the uncertainty in the bead radius, which in theory could be as large as 10–15%. However, it should be noted that in two experiments, very accurate determinations of the bead radius were possible because, by good luck, the bead was larger than one pipette and smaller than the other, even though the pipettes themselves were quite close in size. The pipette radii were determined by insertion of calibrated probes, providing precise limits on possible values of the bead radius in these cases. Inasmuch as the values for k_c determined for these cases were in good agreement with values obtained when the bead radius was determined by direct measurement, we are confident that errors from this particular source were not more than the standard deviation in the calculated values of k_c. Errors due to the use of the Stokes' drag equation for particles that were not spherical or not smooth are more difficult to assess. Nevertheless, the fact that the values of k_c did not vary appreciably when different beads were used suggests that such errors were not large.